

Generalizable Disaster Damage Assessment via Change Detection with Vision Foundation Model

Kyeongjin Ahn
kyeongjin.ahn@kaist.ac.kr
School of Computing, KAIST
Daejeon, Republic of Korea

Sungwon Han
lion4151@kaist.ac.kr
School of Computing, KAIST
Daejeon, Republic of Korea

Sungwon Park
psw0416@kaist.ac.kr
School of Computing, KAIST
Daejeon, Republic of Korea

Jihee Kim
jiheekim@kaist.ac.kr
College of Business, KAIST
Daejeon, Republic of Korea

Sangyoon Park
sangyoon@ust.hk
Division of Social Science, HKUST
Kowloon, Hong Kong

Meeyoung Cha
mia.cha@mpi-sp.org
MPI for Security and Privacy
Bochum, Germany

ABSTRACT

The increasing frequency and intensity of natural disasters demand more sophisticated approaches for rapid and precise damage assessment. To tackle this issue, researchers have developed various methods on disaster benchmark datasets from satellite imagery to aid in detecting disaster damage. However, the diverse nature of geographical landscapes and disasters makes it challenging to apply existing methods to regions unseen during training. We present DAVI (Disaster Assessment with VIision foundation model), which overcomes domain disparities and detects structural damage (e.g., building) without requiring ground-truth labels of the target region. DAVI integrates task-specific knowledge from a model trained on source regions with an image segmentation foundation model to generate pseudo labels of possible damage in the target region. It then employs a two-stage refinement process, targeting both the pixel and overall image, to more accurately pinpoint changes in disaster-struck areas based on before-and-after images. Comprehensive evaluations demonstrate that DAVI achieves exceptional performance across diverse terrains (e.g., USA and Mexico) and disaster types (e.g., wildfires, hurricanes, and earthquakes). This confirms its robustness in assessing disaster impact without dependence on ground-truth labels.

CCS CONCEPTS

• Computing methodologies → Computer vision; Image segmentation; • Applied computing;

KEYWORDS

Disaster assessment; Satellite imagery; Change Detection; Vision Foundation Model; Unsupervised Learning; Label Refinement

Permission to make digital or hard copies of all or part of this work for personal or classroom use is granted without fee provided that copies are not made or distributed for profit or commercial advantage and that copies bear this notice and the full citation on the first page. Copyrights for components of this work owned by others than the author(s) must be honored. Abstracting with credit is permitted. To copy otherwise, or republish, to post on servers or to redistribute to lists, requires prior specific permission and/or a fee. Request permissions from permissions@acm.org.

Conference'24, xxx, xxx

© 2024 Copyright held by the owner/author(s). Publication rights licensed to ACM.
ACM ISBN 978-x-xxxx-xxxx-x/YY/MM
<https://doi.org/XXXXXXXX.XXXXXXX>

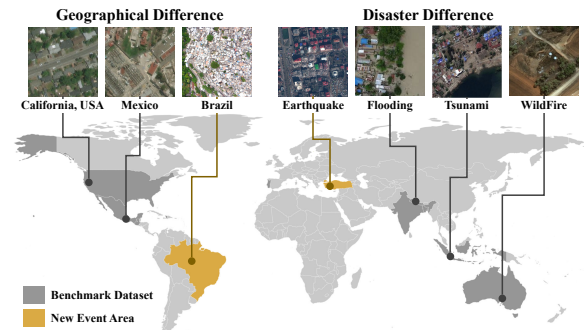


Figure 1: Data challenge. While collaborative efforts are underway to collect datasets on natural disasters, currently the largest benchmark dataset [13] (marked in dark grey) covers only a small part of the world. The areas shown in yellow represent regions with recent disaster events that were not included in the dataset.

ACM Reference Format:

Kyeongjin Ahn, Sungwon Han, Sungwon Park, Jihee Kim, Sangyoon Park, and Meeyoung Cha. 2024. Generalizable Disaster Damage Assessment via Change Detection with Vision Foundation Model. In . ACM, Boise, Idaho, ID, USA, 9 pages. <https://doi.org/XXXXXXXX.XXXXXXX>

1 INTRODUCTION

Natural disasters like wildfires, hurricanes, floods, and earthquakes are becoming more prevalent and severe due to the escalating impacts of climate change [17]. These catastrophic events affect human lives and cause extensive economic loss, necessitating prompt responses in rescue operations and financial assistance. With limited resources available for life-saving relief and funding, assessing disaster damage at a fine-grained infrastructure-level becomes critical for effective resource distribution [9, 10]. Among the efforts, multi-temporal remote sensing images have emerged as a valuable resource for assessing disaster damage, which can cover broad geographic regions at a lower cost relative to traditional ground surveys [1, 13, 14, 34, 46, 49].

Conventional approaches rely on *change detection techniques* that compare the before-and-after visual differences of regional images. For example, methods such as image differentiation [40],

image ratio [39], principal component analysis [19], and change vector analysis [2] can be applied for change detection problems. With the advent of deep learning, more recent approaches spot changes using deep features via thresholding techniques [36], specialized convolution networks [47, 54], and contrastive learning [47].

Nonetheless, the above techniques cannot be readily used in real-world damage assessment due to substantial discrepancies between the available training data (i.e., source data) and the test data (i.e., target data). Figure 1 illustrates this challenge, where the depicted regions appearing in the most extensive disaster benchmark dataset, xBD [13], spanning 45,000 square kilometers of annotated high-resolution satellite images on natural disasters, yet cover a small part of the world. The limited coverage of the benchmark datasets makes it difficult to analyze features of uncovered regions in terms of visual style, including distinct geographical attributes in the regions at an image level. Disaster type is another variation factor in visual features; for example, wildfires can destroy entire buildings, hurricanes may damage only roofs, and floods may engulf structures without causing visible damage. Therefore, *domain adaptation* in images (i.e., shifts in visual styles) is required to address the diverse geographical landscapes, while *adjustment* in the damage prediction criteria (i.e., shift in the decision boundary) is necessary depending on the disaster type.

We present DAVI (**D**isaster **A**ssessment with **V**ision foundation model), which aims to bridge these domain disparities and detect structural damages on buildings and other infrastructure in an unsupervised fashion. This is achieved through the test-time adaptation technique and the vision foundation model. Test-time adaptation is to start from a source model, referring to the model trained on an independent source data, to gradually update the model to be used on the target data without requiring target labels, typically using pseudo labels [6, 24, 30, 42]. We reduce uncertainty arising from domain shifts by minimizing the entropy of pseudo labels. We also integrate pseudo labels with general visual features from the vision foundation model to handle decision boundary shifts. Particularly, we use SAM (Segment Anything Model) [18] that excels at generating semantic masks for various objects, including buildings, roads, vegetation, and water bodies. We show this foundation model is also effective for examining structural damage in disasters.

DAVI refines pseudo labels from the source model through a two-stage process: pixel-level and image-level adjustments. The former utilizes inconsistent change maps from temporally paired images and their augmented ones, while the latter exploits coarse-grained damage presence information. The generated pseudo labels provide supervisory guidance to align our model’s predictions closely with these labels, even without ground-truth labels. Using real-world events across diverse regions and disaster types in the xBD benchmark dataset, we show that DAVI can successfully detect structural damage by adapting to unseen regions, compared to other unsupervised change detection methods and domain adaptation methods.

Our detection method based on the vision foundation model has the potential to aid in the rapid assessment of future disaster damages in uncharted territories. It could serve as a guiding metric, filling the information gap until on-the-ground assessments and detailed surveys become available in the affected areas. We plan to make our code publicly accessible to the research community.

2 RELATED WORK

2.1 Transfer Learning in Change Detection

Transfer learning methods focus on applying a pre-trained model from source data to target data. An advanced version of this is the domain adaptation method, which aims to reduce domain discrepancies between datasets. Given the high cost to acquire ground-truth labels, especially in damage assessment, studies have utilized unsupervised methods. For example, several approaches use pre-trained weights on pretext tasks like segmentation or classification to detect changes in temporally paired images [7, 15, 21, 47, 53]. However, these transfer learning algorithms often assume that the training and test sets are independent and identically distributed (*i.i.d.*), which degrades performance when domain discrepancies exist [33]. Domain adaptation techniques partially address these discrepancies but assume that if the pre-training and fine-tuning tasks share the same class label, the class’s semantic characteristics remain consistent, even if the visual styles differ [24, 41, 42]. For instance, an illustration of an apple and a real-life photo of an apple have different visual styles but share semantic traits that make them recognizable as apples. In our problem setting, however, the significant semantic differences caused by different types of disasters make domain adaptation methods difficult to apply, requiring a decision boundary shift.

2.2 Vision Foundation Model

The advancement of deep neural networks and self-supervised learning has significantly improved vision foundation models (VFM) on large-scale vision data [18, 26, 43–45, 55]. Examples of VFMs for image segmentation include, but are not limited to, CLIPSeg [26], SegGPT [45], SAM [18], and SEEM [55]. These models use visual inputs and prompts—such as text, boxes, points, or masks—to specify target image segmentation and show remarkable adaptability to other domains, such as remote sensing [5, 31], tracking [35, 51], robotics [52], and medical [12, 22, 27, 37, 50], underscoring its effective capability to recognize various visual content. We employ SAM in our change detection method as an assistant due to its simplicity and ease of use. SAM uses an image encoder, a prompt encoder, and a mask decoder. It combines image and prompt embeddings through each encoder to guide object localization, and uses the mask decoder to generate masks from these embeddings for self-annotation.

2.3 Change Detection by Pseudo Labeling

When ground-truth labels are not available, one common strategy to provide supervisory signals is to introduce pseudo labels for training [16, 20, 56]. This pseudo labeling has been used in change detection problems as well to achieve higher accuracy. Examples include Pix4Cap [25], which uses pseudo labels extracted from a pre-trained model to improve the model’s ability to change captioning, and PPL [23], which generates pseudo labels through uncertainty estimation and progressive refinement on hyperspectral images. These change detection methods using pseudo labels rely on self-updating through their own predictions, making implementation easy but accumulating errors over time. In line with this strategy, we utilize pseudo-labeling-based learning but together with an external foundation model and refinement process to reduce error propagation.

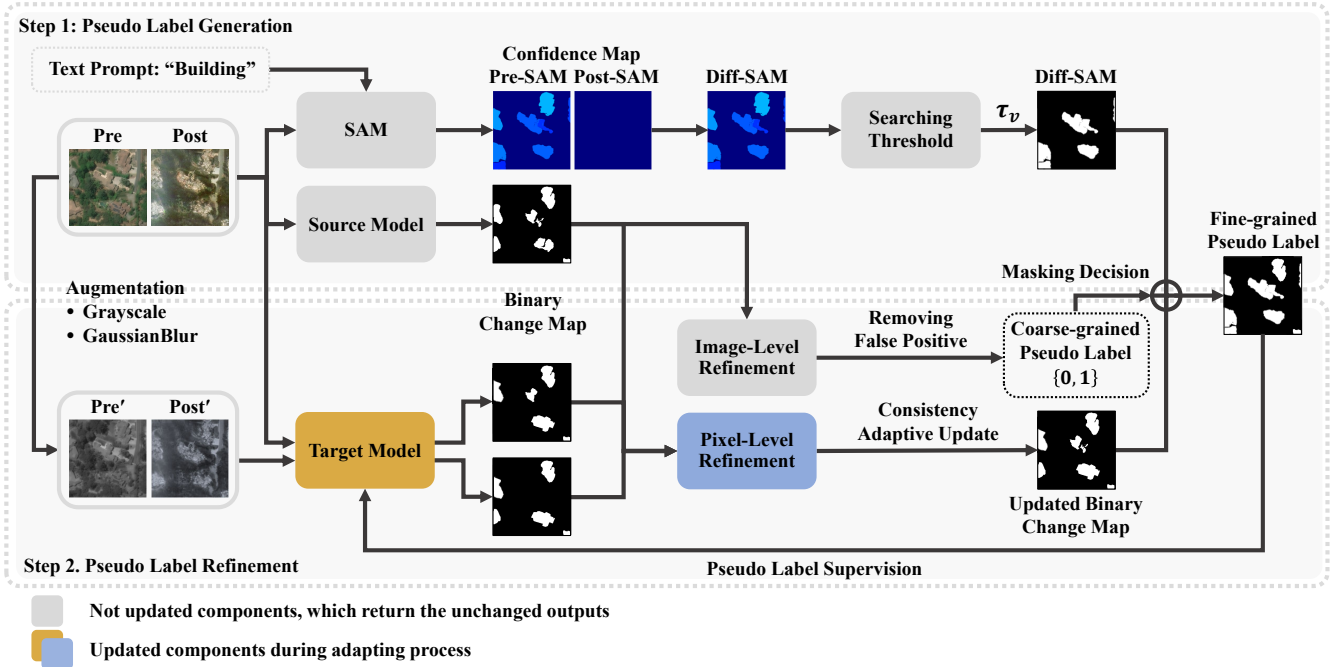


Figure 2: Model architecture. This figure illustrates how pre- and post-disaster images and their augmented versions are processed. The system has two phases: (Step 1) pseudo label generation, which leverages the source model and SAM image segmentation foundation model with a text prompt for generalizability across disaster scenarios, and (Step 2) pseudo label refinement, which involves pixel- and image-level refinement to reduce noise in the fine-grained pseudo label. The final output is a fine-grained pseudo label indicating potential damage.

3 METHODOLOGY

3.1 Problem Formulation

We present an efficient method for disaster assessment, DAVI, which compares pre- and post-disaster images to detect structural damages (e.g., building, infrastructure level). DAVI runs in a test-time adaptation setting, using change detection models trained on unveiled disaster-related data (i.e., source data), adapted to target data. Below is the problem formulation of our setting with an overview of DAVI.

Let us define the source data D_s as unveiled data from the source domain and the target data D_t as veiled one from the target domain. The source data D_s contains temporally paired images and their corresponding ground-truth labels, indicated as $\{\bar{x}_{pre}, \bar{x}_{post}, y\} \in D_s$, where $\bar{x}_{pre} \in \mathbb{R}^{H \times W \times 3}$ represents a pre-disaster image, $\bar{x}_{post} \in \mathbb{R}^{H \times W \times 3}$ represents a post-disaster image, and $y \in \{0, 1\}^{H \times W}$ represents a binary change map, respectively. While the target data D_t consists of temporally paired images, indicated as $\{x_{pre}, x_{post}\} \in D_t$ without access to ground-truth labels. Here, we ensure no overlap between the source and target data. The model trained with the source data (i.e., source model) is denoted as f_0 . The target model, denoted as f , starts from the weight as same as the one from source model f_0 , and is then updated to adapt to the target data during training. Our goal is to address the issue of domain shifts using only the source model and the unlabeled target data, finally providing predictions of the target model f with high accuracy for changed areas in the target data.

To approach this problem, we design pseudo labels $\mathcal{M}_F^* \in \{0, 1\}^{H \times W}$ that accommodate domain shifts across various types of disasters occurring globally. These pseudo labels substitute for the unavailable ground-truth labels in the target data. The intuition behind using pseudo labels is that they provide supervisory guidance, helping the model detect changes in the target data. The generation phase (Step 1) leverages both the source model f_0 with task-specific knowledge based on the source domain and SAM h with task-agnostic knowledge from extensive image corpus. This is followed by a refinement process (Step 2) that improves the accuracy of the pseudo labels by removing noisy parts within them using consistency-based information and coarse-grained information. Ultimately, in addition to supervised learning on the generated pseudo labels, we minimize the entropy of the predictions to learn domain-specific features for the target data. More specifically, our objective to train the target model f can be formulated as:

$$H(\hat{\mathcal{M}}) = - \sum_i \sum_j p^{ij} \log(p^{ij}), \quad (1)$$

where $H(\hat{\mathcal{M}})$ refers to Shannon entropy loss function [38] frequently employed in one of the test-time adaptation approaches, which tries to connect errors arising from the domain discrepancy and the domain shift [41]. Here, $\hat{\mathcal{M}}$ indicates the change maps computed by the target model f , and p^{ij} denotes the probability value within $\hat{\mathcal{M}}$, where (i, j) represents the coordinates of individual pixels. Through this objective function, the target model f eliminates generalization errors by minimizing the entropy of its predictions

on the target data.

$$\mathcal{L} = CE(\mathcal{M}_F^*, \hat{\mathcal{M}}) + \lambda H(\hat{\mathcal{M}}) \quad (2)$$

where \mathcal{M}_F^* is generated fine-grained pseudo labels and λ is an adjusting hyperparameter, which is set to 0.1 as default.

3.2 Step 1: Pseudo Label Generation

We generate the fine-grained pseudo labels \mathcal{M}_F that represent pixel-level binary change maps. This information combines two types of pseudo labels: \mathcal{M}_0 from the source model f_0 and \mathcal{M}_V from SAM, h . This enhances model generalizability across various disaster scenarios by utilizing complementary knowledge. Specifically, while the source model can handle target tasks better, relying solely on the pseudo labels generated by the source model can consistently lead to inaccurate signals due to mismatches between the source and target distributions, ultimately hindering the model's applicability. For example, if the model is excessively overfitted to the source data, it may exhibit undue uncertainty or certainty when applied to the target data. This affects the interpretation and use of the model's predictions, potentially requiring a recalibration of confidence thresholds or adjustments to output probabilities. SAM can analyze visual features across a wide range of domains, as it was trained on billion-scale vision data. By integrating this knowledge with that from the source model, the combined approach can adeptly manage shifts in the decision boundary, thereby improving adaptation in diverse scenarios. Below is our strategy to generate the pseudo labels:

Pseudo label generation with task-specific knowledge. Given the paired images x_{pre} and x_{post} , the source model f_0 predicts the probability p_0^{ij} of the change for each pixel in the change maps $\hat{\mathcal{M}}_0$. (i.e., $\hat{\mathcal{M}}_0^{ij} = p_0^{ij}$)

$$\hat{\mathcal{M}}_0^{ij} = f_0(x_{pre}^{ij}, x_{post}^{ij}) \quad (3)$$

We convert the probability maps $\hat{\mathcal{M}}_0$ into the binary change maps \mathcal{M}_0 as follows:

$$\mathcal{M}_0^{ij} = \begin{cases} 1 & \text{if } p_0^{ij} \geq 0.5 \\ 0 & \text{otherwise} \end{cases}, m_0^{ij} \in \mathcal{M}_0 \quad (4)$$

Pseudo label generation with task-agnostic knowledge. Next, our method segment objects of interest (e.g., buildings, roads, vegetation, and water bodies) based on the vision foundation model like SAM to adjust the source model's pseudo label. It segments specific objects based on text prompts and assigns a confidence score to each object as follows:

$$\hat{\mathcal{W}} = h(x; \text{prompt}), w^{ij} \in \hat{\mathcal{W}} \text{ and } w^{ij} \in [0, 1]. \quad (5)$$

To obtain semantic changes between the paired images, we subtract two segmented maps with confidence scores—specifically, Pre-SAM and Post-SAM. SAM has high confidence for identifying building areas in pre-disaster images, while it would have decreased confidence for damaged building areas in post-disaster images because it lacks the essential features for recognizing buildings. Therefore, we leverage the confidence difference between pre-disaster and post-disaster images as an indicator of building destruction, utilizing SAM h with the text prompt building:

$$\hat{\mathcal{M}}_V^{ij} = \max(0, w_{pre}^{ij} - w_{post}^{ij}), d_v^{ij} \in \hat{\mathcal{M}}_V \quad (6)$$

where $\hat{\mathcal{M}}_V$ represents the confidence difference maps from SAM, referred to as Diff-SAM. We clip the confidence difference maps to be greater than zero to focus on the changes in destruction rather than construction. Then, we transform the confidence difference maps $\hat{\mathcal{M}}_V$ into the binary change maps \mathcal{M}_V as follows:

$$\mathcal{M}_V^{ij} = \begin{cases} 1 & \text{if } d_v^{ij} \geq \tau_v \\ 0 & \text{otherwise} \end{cases} \quad (7)$$

where τ_v represents a threshold determined through optimal threshold searching. For simplicity, we also hereafter refer to \mathcal{M}_V as Diff-SAM. Finally, we combine two binary change maps to generate the fine-grained pseudo labels \mathcal{M}_F as follows:

$$\hat{\mathcal{M}}_F^{ij} = \max_{ij}(\mathcal{M}_0^{ij}, \mathcal{M}_V^{ij}) \quad (8)$$

Searching Optimal Threshold. The threshold τ_v sets the confidence level at which segmentation identifies a building as damaged. The appearance of damaged buildings can vary based on factors such as regional characteristics and the type of disaster, meaning the optimal threshold can also vary accordingly. We determine the optimal threshold by exploring various candidate values that maximize the F1-score between \mathcal{M}_0 and \mathcal{M}_V on the target data D_t . This approach is based on the intuition that finding the precise threshold requires disaster-specific knowledge, which can be aided by the source model, even if it pertains to a different domain.

3.3 Step 2: Pseudo Label Refinement

We refine the fine-grained pseudo labels through in two processes: **Consistency Adaptive Update** and **Coarse-grained Pseudo Labels** to minimize noise in these labels. Despite utilizing knowledge from the source model and SAM, the noise remains in the fine-grained pseudo labels. This issue can be attributed to the distortion of knowledge adapted from the source model to the target distribution due to the domain discrepancy, or to the limited ability of SAM to adequately consider features associated with changes in the target data. We first focus on pixel-level adjustments, targeting areas identified as changed within the fine-grained pseudo labels, guided by confidence-based consistency from the data augmentation strategy. We then engage in image-level adjustments to further enhance noise reduction effectively. This approach concentrates on broadly unchanged information between the paired images, using the coarse-grained pseudo labels from the source model. These labels are used to mask the generated fine-grained pseudo labels, rendering them as all zeros.

Consistency Adaptive Update. Unsupervised or semi-supervised learning can lead to overconfident and poorly calibrated predictions [11, 32]. Consequently, pseudo-labeling-based on confidence scores can be suboptimal. To address this, we propose using inconsistencies arising from data augmentation variations to assess uncertainty for pixel-level refinement. These inconsistencies highlight the model's uncertainty in its decisions. Provided with the paired images x_{pre} and x_{post} , along with their augmented counterparts x'_{pre} and x'_{post} , we adaptively update the predicted binary change maps \mathcal{M}_0 from the source model f_0 using the confidence metrics obtained from these original and augmented paired images. Here, the target model f predicts the probability p^{ij} of the change

for each pixel in the change maps $\hat{\mathcal{M}}$ as same as the source model f_0 .

$$\hat{\mathcal{M}}^{ij} = f(x_{pre}^{ij}, x_{post}^{ij}) \quad (9)$$

Similarly, we obtain additional probability maps from another augmentation, denoted as $\hat{\mathcal{M}}' = f(x'_{pre}, x'_{post})$. Using these probability maps, we then compute mean $\hat{\mathcal{U}}$ and standard deviation \mathcal{S} from $\hat{\mathcal{M}}$ and $\hat{\mathcal{M}}'$ to quantify confidence based on pixel-wise variability. As in Eq. (4), the average probability maps $\hat{\mathcal{U}}$ are converted into the binary change maps \mathcal{U} .

Our refinement operates under the following strategy using $\mu^{ij} \in \mathcal{U}$ and $\sigma^{ij} \in \mathcal{S}$. If variation σ^{ij} is marginal (i.e., it has low uncertainty), we update the value m_0^{ij} in the binary change maps \mathcal{M}_0 from the source model f_0 (see Eq. (4)) to its corresponding value μ^{ij} in the binary change maps \mathcal{U} from the target model f . Conversely, if variation σ^{ij} is high (i.e., it has high uncertainty), we keep the original value m_0^{ij} of the binary change maps \mathcal{M}_0 from the source model f_0 . During each iteration, the binary change maps \mathcal{M}_0 in Eq. (8) are updated, thereby regenerating the fine-grained pseudo labels that reflect the target knowledge. The refining process is described as follows:

$$\mathcal{M}_C^{ij} = \begin{cases} \mu^{ij} & \text{if } \sigma^{ij} < \tau_r \text{ and } m_0^{ij} = 1 \\ m_0^{ij} & \text{otherwise} \end{cases} \quad (10)$$

where \mathcal{M}_C denotes the updated binary change maps, which start from the binary change maps \mathcal{M}_0 of the source model. Here, τ_r is the threshold for pixel update decisions, set to 0.001. Using these updated maps, we can derive the refined fine-grained pseudo labels.

$$\mathcal{M}_F^{ij} = \max_{ij}(\mathcal{M}_C^{ij}, \mathcal{M}_V^{ij}) \quad (11)$$

Coarse-grained Pseudo Labels. We employ the coarse-grained pseudo labels generated from the binary change maps \mathcal{M}_0 of the source model f for the image-level refinement. These labels provide image-level information indicating the absence (0) or presence (1) of changes in the paired images. We use this information to guide the model more effectively by masking the generated fine-grained pseudo labels \mathcal{M}_F in instances where the binary change maps \mathcal{M}_0 show no changes. This refinement process helps suppress false positives (FP) in the fine-grained pseudo labels rather than relying on the unmasked fine-grained pseudo labels. We can formulate the coarse-grained pseudo labels q as follows:

$$q = \begin{cases} 1 & \text{if } \sum_{i,j} m_0^{ij} > 0 \\ 0 & \text{otherwise} \end{cases} \quad (12)$$

Using these labels, we mask the fine-grained pseudo labels $\hat{\mathcal{M}}_F$ as follows:

$$\mathcal{M}_F^* = q \cdot \mathcal{M}_F, \quad m_f^{ij} \in \mathcal{M}_F^* \quad (13)$$

where \mathcal{M}_F^* is the final fine-grained pseudo labels obtained after the image-level refinement. Using these fine-grained pseudo labels, we proceed to train the target model f as follows:

$$CE(\mathcal{M}_F^*, \hat{\mathcal{M}}) = - \sum_i \sum_j m_f^{ij} \log(p^{ij}) \quad (14)$$

4 EXPERIMENTS

4.1 Experimental Setup

Datasets. We evaluate DAVI and other relevant baselines on the well-known change detection benchmark dataset, xBD. This dataset is publicly used for change detection problems and building damage assessment, covering different regions affected by 11 various disasters, such as wildfires, hurricanes, floods, and earthquakes, across more than 45,000 km² of imagery with over 800,000 building annotations. We randomly select source data to train the source model, specifically adopting wildfires in Woolsey, California (USA) and floods in Monsoon (Nepal). This includes 14,048 paired images for wildfires and 9,904 paired images for floods. Our analysis targets explicitly wildfires in Santa Rosa, California (USA), hurricanes in Texas (USA), and earthquakes in Mexico City (Mexico), considering various geographical locations and disaster types for testing purposes. Each test set contains 3,616, 5,104, and 1,936 paired images, respectively. Due to the deviation in disaster level information across different types of disasters, we convert the four-category disaster level information (0: no damage, 1: minor damage, 2: major damage, 3: destroyed) into the binary information (0: no damage, 1: damage) at each pixel within the ground-truth labels. This conversion enables rapid adaptation and efficient resource distribution regardless of the damage criteria.

Baselines. Given that ground-truth labels in target regions are not accessible, we employ four traditional unsupervised change detection baselines—CVA [2], IRMAD [28], PCAKmeans [3], and ISFA [48]—as well as two deep learning-based unsupervised change detection baselines, DCVA [36] and SCCN [54]. CVA is a basic change detection method that computes change intensity and direction for detecting changes. IRMAD is an iterative version of MAD [29], utilizing canonical correlation analysis (CCA) to maximize the correlation between images. PCAKmeans applies k-means clustering after transforming and comparing images in feature space for change detection. ISFA is an iterative version of USFA [48], computing a projection matrix to suppress pseudo change pixels and highlight changed parts. For IRMAD and ISFA, we use 50 and 100 iterations, respectively. DCVA detects changes using global and local thresholding techniques after extracting deep features from pre-trained tasks. SCCN utilizes a symmetric coupling function to enhance feature representation consistency for change detection. We also adopt three relevant domain adaptation baselines—TENT [41], SHOT [24], and CoTTA [42]—and fine-tune them on the same backbone, following the same pre-training process as our proposed method to ensure fair comparisons. TENT updates batch normalization statistics by minimizing entropy on the target data during test time. SHOT leverages pseudo labels to achieve source hypothesis transfer through information maximization. CoTTA utilizes a continual learning approach to avoid catastrophic forgetting in the source domain.

Implementation Details. Our experiments utilize SNUNet-CD [8] as a backbone for both the source model f_0 and the target model f . Additionally, we use BIT-CD [4] as another backbone for both models. These models are designed to predict the change maps $\hat{\mathcal{M}}_0$ and $\hat{\mathcal{M}}$, respectively. Regarding setup details, the batch size is fixed

Table 1: Performance of DAVI and other unsupervised change detection and domain adaptation baselines tested across different geographic regions (USA and Mexico) and disaster types (wildfire, hurricane, and earthquake). The top results are highlighted in bold, and when our method achieves the second-best performance, it is underlined.

Methods	Backbones	Wildfires (California, USA)				Hurricanes (Texas, USA)				Earthquakes (Mexico City, Mexico)			
		Precision	Recall	F1-score	OA	Precision	Recall	F1-score	OA	Precision	Recall	F1-score	OA
Oracle	SNUNet-CD	0.8476	0.7733	0.8087	0.9939	0.8075	0.6190	0.7008	0.9767	0.7852	0.6620	0.7183	0.9996
	BIT-CD	0.8015	0.8272	0.8142	0.9938	0.8162	0.7075	0.7580	0.9801	0.7591	0.7038	0.7304	0.9996
Source	SNUNet-CD	0.4223	0.8386	0.5617	0.9784	0.0466	0.9338	0.0888	0.1542	0.0009	0.9688	0.0017	0.1105
Source†	SNUNet-CD	0.6566	0.8109	0.7256	0.9899	0.6053	0.0414	0.0775	0.9565	0.3024	0.2296	0.2611	0.9990
	BIT-CD	0.8141	0.5033	0.5033	0.9899	0.7317	0.0168	0.0328	0.9563	0.2140	0.0275	0.0487	0.9991
CVA	-	0.0343	0.4583	0.0638	0.7774	0.0527	0.2544	0.0873	0.7653	0.0024	0.6718	0.0047	0.7734
IRMAD	-	0.0290	0.4885	0.0547	0.7090	0.0436	0.2688	0.0750	0.6948	0.0021	0.7833	0.0042	0.6973
PCAKmeans	-	0.0322	0.5501	0.0609	0.7191	0.0306	0.2408	0.0543	0.6299	0.0017	0.6796	0.0034	0.6797
ISFA	-	0.0336	0.4603	0.0626	0.7563	0.0471	0.2163	0.0773	0.7569	0.0028	0.7224	0.0055	0.7750
DCVA	CNN*	0.0320	0.5552	0.0605	0.7028	0.0430	0.2643	0.0740	0.6970	0.0023	0.8394	0.0045	0.6994
SCCN	CNN*	0.0383	0.4821	0.0709	0.7772	0.0500	0.2317	0.0822	0.7551	0.0030	0.7444	0.0061	0.7853
TENT	SNUNet-CD	0.8810	0.1864	0.3077	0.9861	0.5994	0.0053	0.0104	0.9559	0.3565	0.1176	0.1768	0.9991
SHOT	SNUNet-CD	0.6824	0.8025	0.7376	0.9906	0.6057	0.0413	0.0774	0.9565	0.3041	0.2291	0.2613	0.9990
CoTTA	SNUNet-CD	0.8142	0.5150	0.6309	0.9900	0.5621	0.0411	0.0765	0.9563	0.6465	0.0288	0.0552	0.9564
DAVI	SNUNet-CD	0.7206	0.7767	0.7476	0.9913	0.5211	0.3552	0.4225	0.9571	0.3339	0.6094	0.4314	0.9987
	BIT-CD	0.5134	0.8079	0.6278	0.9842	0.6364	0.0803	<u>0.1427</u>	<u>0.9574</u>	0.5102	0.1142	0.1866	0.9992

† This mark indicates the fine-tuned source model, trained on the binary change maps from the pre-trained source model as the fine-grained pseudo labels.

* This backbone is different from the one used in our method.

Table 2: Component analysis, where results after each module: coarse-grained pseudo labels (CG), fine-grained pseudo labels (FG), binary change maps from the source model (SO), SAM’s binary confidence difference maps (DS), and refinement process (RE).

CG	FG			Wildfires (California, USA)			
	SO	DS	RE	Precision	Recall	F1-score	OA
	✓			0.6824	0.8025	0.7376	0.9906
✓	✓			0.7964	0.6903	0.7396	0.9920
		✓		0.7177	0.3486	0.4693	0.9870
✓		✓		0.7504	0.3365	0.4647	0.9872
✓	✓	✓		0.7260	0.7679	0.7463	0.9914
	✓	✓	✓	0.7082	0.7819	0.7432	0.9911
✓	✓	✓	✓	0.7206	0.7767	0.7476	0.9913

at 8 for both the source model and the target model on the SNUNet-CD and BIT-CD backbones. The learning rates for the source and target models on SNUNet-CD are set to $1e-3$ and $1e-5$ respectively, with a weight decay of 0.01. We use the StepLR scheduler with a step size of 8 and a gamma of 0.5. For BIT-CD, the learning rates are set to $1e-2$ for the source model and $1e-4$ for the target model, with a decay ratio of 0.01. All models are trained for 50 epochs using the AdamW optimizer. Additionally, we regulate the degree of adaptation across all experiments by setting λ to 0.1 in Eq. (2).

Performance Evaluation. In all experiments, we used four assessment metrics: macro average of precision, recall, F1-score, and overall accuracy (OA).

Hardware. Our server is equipped with an Intel Xeon Platinum 8268 CPU @ 2.90GHz, 376GB DRAM and 6 NVIDIA V100 GPUs. A single GPU was used for each experiment. Each experiment with

the SNUNet-CD backbone takes an average of 11.5 mins per epoch and those with the BIT-CD backbone take an average of 8.5 mins per epoch across all target data used.

4.2 Comparison with Baseline Models

Table 1 compares DAVI with other relevant baselines. We evaluate both traditional and deep learning-based unsupervised change detection methods, as well as domain adaptation methods. Firstly, traditional methods (i.e., CVA, IRMAD, PCAKmeans, and ISFA) and deep learning-based methods (i.e., DCVA and SCCN) perform poorly overall compared to the proposed method due to their lack of disaster-related knowledge. Although these methods are applied directly to the target data without using a source model trained on change detection tasks and thus are not affected by domain differences, this absence of specific knowledge significantly hinders their effectiveness. Secondly, the baselines (i.e., Source and Source†) that directly utilize the source model benefit from the disaster-related knowledge in the source data, similar to our method, which aids in analyzing the target data. However, their performance declines as domain discrepancies between the source and target increases. For example, while the performance decrease for wildfires is minimal, the performance for other disasters is significantly affected. Thirdly, our method and domain adaptation methods (i.e., TENT, SHOT, and CoTTA) perform better than other methods due to their mechanisms for addressing domain discrepancies. The proposed method, which tackles both visual style shifts and decision boundary shifts, achieves better results across all scenarios than the domain adaptation methods. These results are especially notable for disaster types not included in the source data, such as hurricanes and earthquakes, where SAM proves highly beneficial due to their different inherent semantic characteristics.

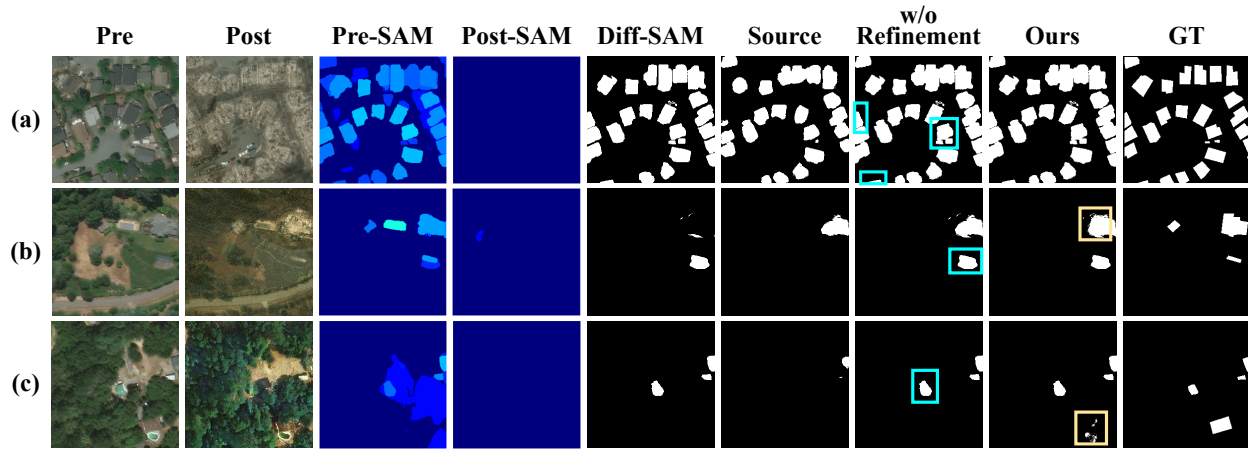


Figure 3: Qualitative analysis with example pseudo labels by DAVI. From left to right, the columns show pre- and post-disaster images, their corresponding confidence maps, confidence difference maps discretized by the optimal threshold, binary change maps from the source model, fine-grained pseudo labels without refinement, our pseudo labels, and ground-truth labels: (a) a case that benefits from segmentation (with the blue box); (b-c) cases that benefits from image segmentation foundation model and refinement process (with the yellow box).

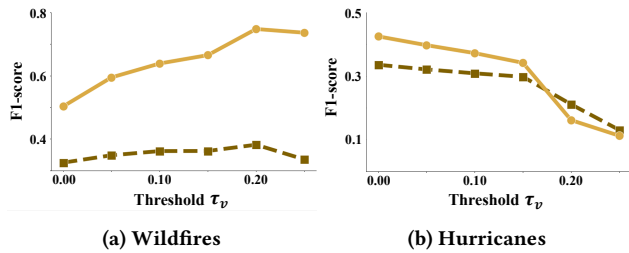


Figure 4: Optimal thresholds for generating binary change maps from SAM. The solid line shows the proposed method’s performance in terms of the F1-score, while the dashed line shows the F1-score between the source model’s binary change maps and SAM’s binary change maps with different thresholds.

4.3 Component Analysis

Component Impact Analysis. We validate the effectiveness of each component of the proposed method through a detailed component analysis in Table 2. Each components contribute to improving the overall performance of our method. In particular, we verify that masking with coarse-grained pseudo labels is effective in all cases. Furthermore, we observe that when the domain difference between the source and target is minimal, using the source is more effective than relying solely on SAM. Nevertheless, incorporating SAM still enhances performance.

Hyperparameter Analysis. Additionally, we provide an analysis to determine the optimal threshold, τ_v in Eq. (7), for generating the binary change maps from the confidence difference maps produced by SAM, as shown in Figure 4. Our results confirm that selecting the threshold based on F1-score criteria by comparing the binary change maps from the source model and SAM with different thresholds yields optimal performance.

4.4 Qualitative Analysis

We also qualitatively analyze the impact of each component within DAVI on wildfires. Figure 3 presents examples showing how our method benefits from the source model and SAM, refining the pseudo labels based on target model outputs. The blue boxes highlight areas where SAM has positively influenced detection by identifying areas missed by the source model. The yellow boxes show areas improved through the refinement process, either by correcting recognized buildings (b) or identifying new structures (c).

5 CONCLUSION

This paper investigated the test-time adaptation strategy and the vision foundation model for detecting fine-grained structural disaster damages over unseen regions. To refine these pseudo labels at two levels: pixel-level and image-level adjustments, we exploit variation maps from the target model along with coarse-grained pseudo labels. Our experimental results based on the real-world disaster benchmark dataset confirm considerable improvements in damage detection compared to other baselines. Our model could pinpoint structural damage with high accuracy by combining the change detection algorithm that systematically analyzes pre- and post-disaster imagery, as well as the vision foundation model’s rich visual contextual data.

Broader Impact. Our study showed the capability of a new change detection model to handle domain shift challenges in disaster mapping and accurately assess structural damages in unseen regions without ground-truth labels. Our model’s enhanced generalizability across geography and disaster types means that it can be used to assist organizations and low-income countries in improving their ability to mitigate natural disaster damage and deliver humanitarian aid. To maximize the research impact, we plan to share our code and processed dataset with international researchers and governments. We hope this application helps develop relevant policies to minimize the negative impacts in global disaster-prone areas.

REFERENCES

- [1] Yanbing Bai, Junjie Hu, Jinhua Su, Xing Liu, Haoyu Liu, Xianwen He, Shengwang Meng, Erick Mas, and Shunichi Koshimura. 2020. Pyramid pooling module-based semi-siamese network: A benchmark model for assessing building damage from xBD satellite imagery datasets. *Remote Sensing* 12, 24 (2020), 4055.
- [2] Lorenzo Bruzzone and Diego F Prieto. 2000. Automatic analysis of the difference image for unsupervised change detection. *IEEE Transactions on Geoscience and Remote Sensing* 38, 3 (2000), 1171–1182.
- [3] Turgay Celik. 2009. Unsupervised change detection in satellite images using principal component analysis and k -means clustering. *IEEE Geoscience and Remote Sensing Letters* 6, 4 (2009), 772–776.
- [4] Hao Chen, Zipeng Qi, and Zhenwei Shi. 2021. Remote sensing image change detection with transformers. *IEEE Transactions on Geoscience and Remote Sensing* 60 (2021), 1–14.
- [5] Keyan Chen, Chenyang Liu, Hao Chen, Haotian Zhang, Wenyuan Li, Zhengxia Zou, and Zhenwei Shi. 2024. RSPrompter: Learning to prompt for remote sensing instance segmentation based on visual foundation model. *IEEE Transactions on Geoscience and Remote Sensing* (2024).
- [6] Weijie Chen, LuoJun Lin, Shicai Yang, Di Xie, Shiliang Pu, and Yueting Zhuang. 2022. Self-supervised noisy label learning for source-free unsupervised domain adaptation. In *2022 IEEE/RSJ International Conference on Intelligent Robots and Systems*. IEEE, 10185–10192.
- [7] Kevin Louis de Jong and Anna Sergeevna Bosman. 2019. Unsupervised change detection in satellite images using convolutional neural networks. In *2019 International Joint Conference on Neural Networks*. IEEE, 1–8.
- [8] Sheng Fang, Kaiyu Li, Jinyuan Shao, and Zhe Li. 2021. SNUNet-CD: A densely connected Siamese network for change detection of VHR images. *IEEE Geoscience and Remote Sensing Letters* 19 (2021), 1–5.
- [9] Frank Fiedrich, Fritz Gehbauer, and Uwe Rickers. 2000. Optimized resource allocation for emergency response after earthquake disasters. *Safety science* 35, 1-3 (2000), 41–57.
- [10] Christopher B Field, Vicente Barros, Thomas F Stocker, and Qin Dahe. 2012. *Managing the risks of extreme events and disasters to advance climate change adaptation: special report of the intergovernmental panel on climate change*. Cambridge University Press.
- [11] Mingfei Gao, Zizhao Zhang, Guo Yu, Sercan Ö Arık, Larry S Davis, and Tomas Pfister. 2020. Consistency-based semi-supervised active learning: Towards minimizing labeling cost. In *Computer Vision—ECCV 2020: 16th European Conference, Glasgow, UK, August 23–28, 2020, Proceedings, Part X 16*. Springer, 510–526.
- [12] Shizhan Gong, Yuan Zhong, Wenao Ma, Jinpeng Li, Zhao Wang, Jingyang Zhang, Pheng-Ann Heng, and Qi Dou. 2023. 3dsam-adaptor: Holistic adaptation of sam from 2d to 3d for promptable medical image segmentation. *arXiv preprint arXiv:2306.13465* (2023).
- [13] Ritwik Gupta, Bryce Goodman, Nirav Patel, Ricky Hosfelt, Sandra Sajeer, Eric Heim, Jigar Doshi, Keane Lucas, Howie Choset, and Matthew Gaston. 2019. Creating xBD: A dataset for assessing building damage from satellite imagery. In *Proceedings of the IEEE/CVF Conference on Computer Vision and Pattern Recognition Workshops*. 10–17.
- [14] Rohit Gupta and Mubarak Shah. 2021. Rescuenet: Joint building segmentation and damage assessment from satellite imagery. In *2020 25th International Conference on Pattern Recognition*. IEEE, 4405–4411.
- [15] Bin Hou, Yunhong Wang, and Qingjie Liu. 2017. Change detection based on deep features and low rank. *IEEE Geoscience and Remote Sensing Letters* 14, 12 (2017), 2418–2422.
- [16] Meiqi Hu, Chen Wu, Bo Du, and Liangpei Zhang. 2023. Binary change guided hyperspectral multiclass change detection. *IEEE Transactions on Image Processing* 32 (2023), 791–806.
- [17] IPCC. 2022. *Climate Change 2022: Impacts, Adaptation, and Vulnerability*. Cambridge University Press, In Press.
- [18] Alexander Kirillov, Eric Mintun, Nikhila Ravi, Hanzi Mao, Chloe Rolland, Laura Gustafson, Tete Xiao, Spencer Whitehead, Alexander C Berg, Wan-Yen Lo, et al. 2023. Segment anything. In *Proceedings of the IEEE/CVF International Conference on Computer Vision*. 4015–4026.
- [19] Ludmila I Kuncheva and William J Faithfull. 2013. PCA feature extraction for change detection in multidimensional unlabeled data. *IEEE Transactions on Neural Networks and Learning Systems* 25, 1 (2013), 69–80.
- [20] Dong-Hyun Lee et al. 2013. Pseudo-label: The simple and efficient semi-supervised learning method for deep neural networks. In *Workshop on Challenges in Representation Learning, ICLR*, Vol. 3. Atlanta, 896.
- [21] Marrit Leenstra, Diego Marcos, Francesca Bovolo, and Devis Tuia. 2021. Self-supervised pre-training enhances change detection in Sentinel-2 imagery. In *Pattern Recognition, ICPRI International Workshops and Challenges: Virtual Event, January 10–15, 2021, Proceedings, Part VII*. Springer, 578–590.
- [22] Wenhui Lei, Xu Wei, Xiaofan Zhang, Kang Li, and Shaoting Zhang. 2023. Medlsam: Localize and segment anything model for 3d medical images. *arXiv preprint arXiv:2306.14752* (2023).
- [23] Qiuxia Li, Tingkui Mu, Abudusalamu Tuniyazi, Qiujiu Yang, and Haishan Dai. 2024. Progressive pseudo-label framework for unsupervised hyperspectral change detection. *International Journal of Applied Earth Observation and Geoinformation* 127 (2024), 103663.
- [24] Jian Liang, Dapeng Hu, and Jiashi Feng. 2020. Do we really need to access the source data? source hypothesis transfer for unsupervised domain adaptation. In *International Conference on Machine Learning*. PMLR, 6028–6039.
- [25] Chenyang Liu, Keyan Chen, Zipeng Qi, Haotian Zhang, Zhengxia Zou, and Zhenwei Shi. 2023. Pixel-Level Change Detection Pseudo-Label Learning for Remote Sensing Change Captioning. *arXiv preprint arXiv:2312.15311* (2023).
- [26] Timo Lüddecke and Alexander Ecker. 2022. Image segmentation using text and image prompts. In *Proceedings of the IEEE/CVF Conference on Computer Vision and Pattern Recognition*. 7086–7096.
- [27] Jun Ma, Yuting He, Feifei Li, Lin Han, Chenyu You, and Bo Wang. 2024. Segment anything in medical images. *Nature Communications* 15, 1 (2024), 654.
- [28] Allan Aasbjerg Nielsen. 2007. The regularized iteratively reweighted MAD method for change detection in multi-and hyperspectral data. *IEEE Transactions on Image processing* 16, 2 (2007), 463–478.
- [29] Allan A Nielsen, Knut Conradsen, and James J Simpson. 1998. Multivariate alteration detection (MAD) and MAF postprocessing in multispectral, bitemporal image data: New approaches to change detection studies. *Remote Sensing of Environment* 64, 1 (1998), 1–19.
- [30] Shuaicheng Niu, Jiayang Wu, Yifan Zhang, Yaofu Chen, Shijian Zheng, Peilin Zhao, and Mingkui Tan. 2022. Efficient test-time model adaptation without forgetting. In *International Conference on Machine Learning*. PMLR, 16888–16905.
- [31] Lucas Prado Osco, Qiusheng Wu, Eduardo Lopes de Lemos, Wesley Nunes Gonçalves, Ana Paula Marques Ramos, Jonathan Li, and José Marcato Junior. 2023. The segment anything model (sam) for remote sensing applications: From zero to one shot. *International Journal of Applied Earth Observation and Geoinformation* 124 (2023), 103540.
- [32] Sungwon Park, Sungwon Han, Sundong Kim, Danu Kim, Sungkyu Park, Seunghoon Hong, and Meeyoung Cha. 2021. Improving unsupervised image clustering with robust learning. In *Proceedings of the IEEE/CVF Conference on Computer Vision and Pattern Recognition*. 12278–12287.
- [33] Novi Patricia and Barbara Caputo. 2014. Learning to learn, from transfer learning to domain adaptation: A unifying perspective. In *Proceedings of the IEEE Conference on Computer Vision and Pattern Recognition*. 1442–1449.
- [34] Abhishek V Potnis, Rajat C Shinde, Surya S Durbha, and Kuldeep R Kurte. 2019. Multi-class segmentation of urban floods from multispectral imagery using deep learning. In *IGARSS 2019-2019 IEEE International Geoscience and Remote Sensing Symposium*. IEEE, 9741–9744.
- [35] Frano Rajič, Lei Ke, Yu-Wing Tai, Chi-Keung Tang, Martin Danelljan, and Fisher Yu. 2023. Segment anything meets point tracking. *arXiv preprint arXiv:2307.01197* (2023).
- [36] Sudipan Saha, Francesca Bovolo, and Lorenzo Bruzzone. 2019. Unsupervised deep change vector analysis for multiple-change detection in VHR images. *IEEE Transactions on Geoscience and Remote Sensing* 57, 6 (2019), 3677–3693.
- [37] Tal Shaharabany, Aviad Dahan, Raja Giryes, and Lior Wolf. 2023. Autosam: Adapting sam to medical images by overloading the prompt encoder. *arXiv preprint arXiv:2306.06370* (2023).
- [38] Claude Elwood Shannon. 1948. A mathematical theory of communication. *The Bell System Technical Journal* 27, 3 (1948), 379–423.
- [39] Kurt Skiftstad and Ramesh Jain. 1989. Illumination independent change detection for real world image sequences. *Computer Vision, Graphics, and Image Processing* 46, 3 (1989), 387–399.
- [40] Pierre-Luc St-Charles, Guillaume-Alexandre Bilodeau, and Robert Bergevin. 2014. SuSENSE: A universal change detection method with local adaptive sensitivity. *IEEE Transactions on Image Processing* 24, 1 (2014), 359–373.
- [41] Dequan Wang, Evan Shelhamer, Shaoteng Liu, Bruno Olshausen, and Trevor Darrell. 2020. Tent: Fully Test-Time Adaptation by Entropy Minimization. In *International Conference on Learning Representations*.
- [42] Qin Wang, Olga Fink, Luc Van Gool, and Dengxin Dai. 2022. Continual test-time domain adaptation. In *Proceedings of the IEEE/CVF Conference on Computer Vision and Pattern Recognition*. 7201–7211.
- [43] Wenhui Wang, Zhe Chen, Xiaokang Chen, Jiannan Wu, Xizhou Zhu, Gang Zeng, Ping Luo, Tong Lu, Jie Zhou, Yu Qiao, et al. 2024. Visionllm: Large language model is also an open-ended decoder for vision-centric tasks. *Advances in Neural Information Processing Systems* 36 (2024).
- [44] Xinlong Wang, Wen Wang, Yue Cao, Chunhua Shen, and Tiejun Huang. 2023. Images speak in images: A generalist painter for in-context visual learning. In *Proceedings of the IEEE/CVF Conference on Computer Vision and Pattern Recognition*. 6830–6839.
- [45] Xinlong Wang, Xiaosong Zhang, Yue Cao, Wen Wang, Chunhua Shen, and Tiejun Huang. 2023. Seggpt: Segmenting everything in context. *arXiv preprint arXiv:2304.03284* (2023).
- [46] Ethan Weber and Hassan Kané. 2020. Building disaster damage assessment in satellite imagery with multi-temporal fusion. *arXiv preprint arXiv:2004.05525* (2020).

- [47] Chen Wu, Hongruixuan Chen, Bo Du, and Liangpei Zhang. 2021. Unsupervised change detection in multitemporal VHR images based on deep kernel PCA convolutional mapping network. *IEEE Transactions on Cybernetics* 52, 11 (2021), 12084–12098.
- [48] Chen Wu, Bo Du, and Liangpei Zhang. 2013. Slow feature analysis for change detection in multispectral imagery. *IEEE Transactions on Geoscience and Remote Sensing* 52, 5 (2013), 2858–2874.
- [49] Chuyi Wu, Feng Zhang, Junshi Xia, Yichen Xu, Guoqing Li, Jibo Xie, Zhenhong Du, and Renyi Liu. 2021. Building damage detection using U-Net with attention mechanism from pre-and post-disaster remote sensing datasets. *Remote Sensing* 13, 5 (2021), 905.
- [50] Junde Wu, Rao Fu, Huihui Fang, Yuanpei Liu, Zhaowei Wang, Yanwu Xu, Yueming Jin, and Tal Arbel. 2023. Medical sam adapter: Adapting segment anything model for medical image segmentation. *arXiv preprint arXiv:2304.12620* (2023).
- [51] Jinyu Yang, Mingqi Gao, Zhe Li, Shang Gao, Fangjing Wang, and Feng Zheng. 2023. Track anything: Segment anything meets videos. *arXiv preprint arXiv:2304.11968* (2023).
- [52] Jiange Yang, Wenhui Tan, Chuhao Jin, Bei Liu, Jianlong Fu, Ruihua Song, and Limin Wang. 2023. Pave the way to grasp anything: Transferring foundation models for universal pick-place robots. *arXiv preprint arXiv:2306.05716* (2023).
- [53] Min Zhang and Wenzhong Shi. 2020. A feature difference convolutional neural network-based change detection method. *IEEE Transactions on Geoscience and Remote Sensing* 58, 10 (2020), 7232–7246.
- [54] Wei Zhao, Zhirui Wang, Maoguo Gong, and Jia Liu. 2017. Discriminative feature learning for unsupervised change detection in heterogeneous images based on a coupled neural network. *IEEE Transactions on Geoscience and Remote Sensing* 55, 12 (2017), 7066–7080.
- [55] Xueyan Zou, Jianwei Yang, Hao Zhang, Feng Li, Linjie Li, Jianfeng Wang, Lijuan Wang, Jianfeng Gao, and Yong Jae Lee. 2024. Segment everything everywhere all at once. *Advances in Neural Information Processing Systems* 36 (2024).
- [56] Yuliang Zou, Zizhao Zhang, Han Zhang, Chun-Liang Li, Xiao Bian, Jia-Bin Huang, and Tomas Pfister. 2020. Pseudoseg: Designing pseudo labels for semantic segmentation. *arXiv preprint arXiv:2010.09713* (2020).